# Enhancement of nonclassical Raman light intensity by plasmonic nanoantenna

V. Yu. Shishkov,[1,2,3] E. S. Andrianov,[1,2,3] A. A. Pukhov,[1,2,3] and A. P. Vinogradov[1,2,3]
[1]*Dukhov Research Institute of Automatics (VNIIA), 22 Sushchevskaya, Moscow 127055, Russia*
[2]*Moscow Institute of Physics and Technology, 9 Institutskiy pereulok, Dolgoprudny 141700, Moscow region, Russia*
[3]*Institute for Theoretical and Applied Electromagnetics, 13 Izhorskaya, Moscow 125412, Russia*

(Received 4 November 2020; accepted 8 January 2021; published 26 January 2021)

As is well known, light arising from Raman scattering on molecules shows nonclassical mutual correlations between the Stokes and anti-Stokes components. However, the practical use of nonclassical Raman light is limited, due to its low intensity. The Raman signal can be enhanced in surface-enhanced Raman scattering (SERS) experiments by placing Raman active molecules near a plasmonic nanoantenna, due to the Purcell effect. Since the main contribution to emission in SERS experiments is re-emitted light from the plasmonic nanoantenna with no nonclassical correlations, the question arises as to whether it is possible to simultaneously amplify the Raman signal and preserve the nonclassical correlations. In this work, we give a positive answer to this question. We show that plasmonic nanoantennas can be used to enhance the nonclassical light intensity. We demonstrate that the main factor causing deterioration of the cross correlations of SERS light is the fluorescent background of the plasmonic nanoantenna. We analyze the way in which the geometry of a plasmonic nanoantenna affects the nonclassical cross correlations of the Raman light, and show that there is an optimal size of plasmonic nanoantenna that both increases the Raman signal and preserves the nonclassical correlations of the light at the level of a single molecule. The obtained results pave the way for the creation of sources with controlled intensity and a degree of nonclassicality.

DOI: 10.1103/PhysRevA.103.013725

## I. INTRODUCTION

It was recently shown experimentally that in spontaneous Raman scattering, Stokes and anti-Stokes photons are produced in pairs and exhibit nonclassical correlations [1–6]. This means that the product of the second-order coherence functions at the Stokes and anti-Stokes frequencies, $g^{(2)}_{\mathrm{St,St}} = \langle \hat{a}^\dagger_{\mathrm{St}} \hat{a}^\dagger_{\mathrm{St}} \hat{a}_{\mathrm{St}} \hat{a}_{\mathrm{St}} \rangle / \langle \hat{a}^\dagger_{\mathrm{St}} \hat{a}_{\mathrm{St}} \rangle^2$ and $g^{(2)}_{a\mathrm{St},a\mathrm{St}} = \langle \hat{a}^\dagger_{a\mathrm{St}} \hat{a}^\dagger_{a\mathrm{St}} \hat{a}_{a\mathrm{St}} \hat{a}_{a\mathrm{St}} \rangle / \langle \hat{a}^\dagger_{a\mathrm{St}} \hat{a}_{a\mathrm{St}} \rangle^2$, is less than the mutual second-order coherence function, $g^{(2)}_{\mathrm{St},a\mathrm{St}} = \langle \hat{a}^\dagger_{\mathrm{St}} \hat{a}^\dagger_{a\mathrm{St}} \hat{a}_{a\mathrm{St}} \hat{a}_{\mathrm{St}} \rangle / \langle \hat{a}^\dagger_{a\mathrm{St}} \hat{a}_{a\mathrm{St}} \rangle \langle \hat{a}^\dagger_{\mathrm{St}} \hat{a}_{\mathrm{St}} \rangle$, i.e., $g^{(2)}_{\mathrm{St,St}} g^{(2)}_{a\mathrm{St},a\mathrm{St}} < (g^{(2)}_{\mathrm{St},a\mathrm{St}})^2$, indicating that the classical Cauchy-Schwarz inequality is violated [7]. The pairwise production of Stokes and anti-Stokes photons has been demonstrated in experiments with diamond [1–3], water [4,5], organic molecules [6], and several other substances [5]. Paired Stokes and anti-Stokes photons can be used, for example, in ghost imaging [8–11]. The possibility of generating paired photons is also important in applications [12] such as controlling the statistics of anti-Stokes photons [13–16], increasing the contrast of two-photon interferometry [17,18], increasing the contrast of Hong-Ou-Mandel interference [19,20], and enhancing the contrast of measurements of photon entanglement [21].

The intensity of the paired Stokes and anti-Stokes photons arising from spontaneous Raman scattering is low, which limits the range of practical applications. One of the most common ways to increase the intensity is to use plasmonic nanoantennas [22–29]. When Raman-active molecules are placed near a plasmonic nanoantenna, the intensity of spontaneous Raman scattering can be increased by a factor of up to $10^6$ [30–40]. In this case, the intensity is enhanced due to the fact that the scattered light is emitted predominantly by the plasmonic nanoantenna [36] which has a larger dipole moment than a single molecule. For this reason, the Stokes and anti-Stokes light mixes with the luminescent background of the plasmonic nanoantenna [41–47]. In many cases, the intensity of the luminescence background of the nanoantenna is comparable to the intensity of the Raman scattered signal [48]. Nevertheless, this is not critical for spectroscopic applications since there are several efficient ways of subtracting the photoluminescence background [49–53]. However, the question remains as to whether this photoluminescent background causes the deterioration of the nonclassical cross correlations of Stokes and anti-Stokes light. Studies of the influence of plasmonic nanoantennas on the statistical properties of light sources show that as a rule, they have a negative impact on the statistics of the emitted light [54–60]. For example, it has been shown that plasmonic nanoantennas retain the single-photon properties of atoms only at strong coupling and low pumping [60]. At the same time, the question of the effect of the photoluminescent background on the nonclassical cross correlations of Raman light remains open.

In this work, we address this problem and study the effect of a plasmonic nanoantenna on the cross correlations of Stokes and anti-Stokes light from molecules placed in the vicinity of a plasmonic nanoantenna. We consider a regime with a large Purcell factor [61], in which molecules are emitted mainly via the plasmonic nanoantenna. Based on

 

these conditions, we obtain an analytical expression for the cross correlations of the intensities of the Stokes and anti-Stokes components of the spectrum, and show that the main destructive factor affecting the cross correlations of Stokes and anti-Stokes light is the photoluminescent background of the plasmonic nanoantenna. We analyze ways of optimizing the geometry of the plasmonic nanoantenna in order to simultaneously amplify the Raman signal and maintain the nonclassical cross correlations. We find that there is an optimal nanoparticle size at which we can achieve an increase in the radiation intensity typical of surface-enhanced Raman scattering (SERS) experiments, while preserving the nonclassical light correlations at the level of an isolated molecule. This result opens up possibilities for the implementation of spontaneous Raman scattering in nonclassical light sources.

## II. DESCRIPTION OF THE MODEL

We consider Raman active molecules placed near a plasmonic nanoantenna. The entire system is illuminated by an external coherent light source, and the external electromagnetic field interacts with the electrons of the molecules and plasmonic nanoantenna and induces their dipole moments [7,62]. Underline that the external source of the electromagnetic field does not directly excite vibrations of the nuclei of molecules; instead, electrons of the molecules interact parametrically with the vibrations of the nuclei [63–70]. The complete Hamiltonian for the system under consideration, written using the rotating-wave approximation, has the form [71,72]

$$\begin{aligned}\hat{H}_{\rm S} &= \hbar\omega_\sigma \sum_j \hat{\sigma}_j^\dagger \hat{\sigma}_j + \hbar\omega_{\rm v} \sum_j \hat{b}_j^\dagger \hat{b}_j + \hbar g \sum_j \hat{\sigma}_j^\dagger \hat{\sigma}_j (\hat{b}_j^\dagger + \hat{b}_j) \\ &+ \hbar \sum_j \Omega_j (\hat{\sigma}_j^\dagger e^{-i\omega_\Omega t} + \hat{\sigma}_j e^{i\omega_\Omega t}) \\ &+ \hbar\Omega_{\rm pl}(\hat{a}^\dagger e^{-i\omega_\Omega t} + \hat{a} e^{i\omega_\Omega t}) + \hbar\omega_a \hat{a}^\dagger \hat{a} \\ &+ \hbar \sum_j \Omega_{{\rm R}j} (\hat{\sigma}_j^\dagger \hat{a} + \hat{\sigma}_j \hat{a}^\dagger). \end{aligned} \tag{1}$$

Here, we consider the electronic subsystem of molecules as a two-level system, with a transition energy $\hbar\omega_\sigma$ for each molecule and a lowering operator $\hat{\sigma}_j$ for the $j$ th molecule. Vibrations of the nuclei of a molecule are considered using a harmonic approximation, with a natural vibration frequency $\omega_{\rm v}$ and a lowering operator $\hat{b}_j$. We also denote the resonance frequency of the plasmonic nanoantenna as $\omega_a$ and the lowering operator for the near electric field of the plasmonic nanoantenna as $\hat{a}$ (for more details of the quantization of the near field of subwavelength plasmonic structures, see [73,74]). In terms of their physical meanings, the operators $\hat{\sigma}_j$ and $\hat{a}$ are dimensionless operators of the dipole moment of the molecule and the plasmonic nanoantenna, respectively. They are connected with their dimensional dipole moments $\hat{d}_{{\rm mol}j}$ and $\hat{d}_{\rm pl}$ through the expressions $\hat{d}_{{\rm mol}j} = d_{\rm eg}(\hat{\sigma}_j^\dagger + \hat{\sigma}_j)$ and $\hat{d}_{\rm pl} = d_{\rm pl}(\hat{a} + \hat{a}^\dagger)$, respectively, where $d_{\rm eg}$ and $d_{\rm pl}$ are the matrix elements of the corresponding dipole moments. Similarly, the operator of the vibration amplitude of the nucleus of the $j$ th molecule $\hat{x}_j$ can be expressed in terms of the operator $\hat{b}_j$, according to $\hat{x}_j = x(\hat{b}_j^\dagger + \hat{b}_j)$, where $x = \sqrt{\hbar/2m\omega_{\rm v}}$ is the quantum of the vibration amplitude of the nuclei of the molecule. Hence, the meaning of the operator $\hat{b}$ is a dimensionless amplitude of vibration. The quantity $\Omega_{{\rm R}j} = -E_{{\rm pl}j} d_{\rm eg}/\hbar$ is the constant of the interaction between the plasmon and the electron subsystem of the molecule, where $E_{\rm pl}$ is the *plasmonic nanoantenna* electric field strength per one plasmon at the point of location of the $j$ th molecule (for more details, see [75]). The quantity $\Omega_j = -E_{{\rm ext}j} d_{\rm eg}/\hbar$ is the interaction constant between the *external field* at the point of location of the $j$ th molecule and the dipole moment of the transition of the electronic subsystem of the molecule, and $\omega_\Omega$ is the frequency of the external field. The quantity $\Omega_{\rm pl} = -d_{\rm pl} E_{\rm ext\_pl}/\hbar$ determines the constant of interaction of the external field with the plasmonic nanoantenna, where $E_{\rm ext\_pl}$ is the amplitude of the external field at the location of the plasmonic nanoantenna. The constant $g$ is the interaction constant of the electronic subsystem of the molecule with its vibrational subsystem.

The equations for the operators $\hat{b}_j$, $\hat{\sigma}_j$ and $\hat{a}$ are obtained from the Heisenberg equation $d\hat{A}/dt = i[\hat{H},\hat{A}]$ (below $\hat{A} = \hat{a},\hat{\sigma}_j,\hat{b}_j$) using the Hamiltonian (1) and the commutation relations $[\hat{a},\hat{a}^\dagger] = \hat{1}$, $[\hat{b}_i,\hat{b}_j^\dagger] = \hat{1}\delta_{ij}$, $[\hat{\sigma}_i,\hat{\sigma}_j^\dagger] = (1 - 2\hat{\sigma}_j^\dagger\hat{\sigma}_j)\delta_{ij}$. In addition, we will take into account the losses in the vibrational and the electronic subsystem of the molecules and the plasmonic nanoantenna. To do this, we add to the Heisenberg equations relaxation terms of the form $-\gamma_A A$ and noise terms $\hat{F}_A(t)$, connected by the fluctuation-dissipation theorem. As a result, we obtain the following system of Heisenberg-Langevin equations (see also [76,77]):

$$\begin{aligned} d\hat{\sigma}_j/dt &= (-i\omega_\sigma - \gamma_\sigma)\hat{\sigma}_j + i(2\hat{\sigma}_j^\dagger\hat{\sigma}_j - 1) \\ &\quad \times (\Omega_j e^{-i\omega_\Omega t} + i\Omega_{{\rm R}j} a) - ig\hat{\sigma}_j(\hat{b}_j^\dagger + \hat{b}_j) + \hat{F}_{\sigma_j}(t) \end{aligned} \tag{2}$$

$$d\hat{a}/dt = (-i\omega_a - \gamma_a)\hat{a} - i\sum_j \Omega_{{\rm R}j}\hat{\sigma}_j - i\Omega_{\rm pl} e^{-i\omega_\Omega t} + \hat{F}_a(t) \tag{3}$$

$$d\hat{b}_j/dt = (-i\omega_{\rm v} - \gamma_{\rm v})\hat{b}_j - ig\hat{\sigma}_j^\dagger\hat{\sigma}_j + \hat{F}_{b_j}(t), \tag{4}$$

where $\gamma_\sigma$, $\gamma_a$, and $\gamma_{\rm v}$ are the decay rates of the dipole moment of molecules (i.e., dephasing rate), the dipole moment of the plasmonic nanoantenna, and the amplitude of oscillations of the nuclei of molecules, respectively. $\hat{F}_{\sigma_j}(t)$, $\hat{F}_a(t)$, and $\hat{F}_{b_j}(t)$ represent the noises in the electronic subsystem of the $j$ th molecule, plasmon nanoantenna, and the vibrational degree of freedom of the $j$ th molecule, respectively.

As noted above, the correlation properties of the noises in the vibrational and electronic subsystems are related to the relaxation rates according to the fluctuation-dissipation theorem [62,78]: $\langle \hat{F}_{\sigma_j}^\dagger(t)\hat{F}_{\sigma_i}(t')\rangle = \gamma_\sigma\langle\hat{\sigma}_j^\dagger\hat{\sigma}_j\rangle\delta_{ij}\delta(t-t')$, $\langle \hat{F}_{b_i}^\dagger(t)\hat{F}_{b_j}(t')\rangle = \gamma_{\rm v}\bar{n}_{\rm v}^{\rm th}\delta_{ij}\delta(t-t')$, where $\bar{n}_{\rm v}^{\rm th} = [\exp(\hbar\omega_{\rm v}/k_{\rm B}T) - 1]^{-1}$ is the average number of quanta in the reservoir, which gives the relaxation of vibration of the molecular nuclei. The quantity $\langle\hat{\sigma}_j^\dagger\hat{\sigma}_j\rangle$ determines the amplitude of the noise in the electronic subsystem, and can be estimated as $\langle\hat{\sigma}_j^\dagger\hat{\sigma}_j\rangle \propto 1/|\omega_\Omega - \omega_\sigma|^2 \sim 1/{\omega_\sigma}^2$. Since we are considering the case of a large detuning, $|\omega_\Omega - \omega_\sigma| \sim \omega_\sigma \gg \Omega_{{\rm R}j}, \Omega_j$, then the value $\langle\hat{\sigma}_j^\dagger\hat{\sigma}_j\rangle \ll 1$, and

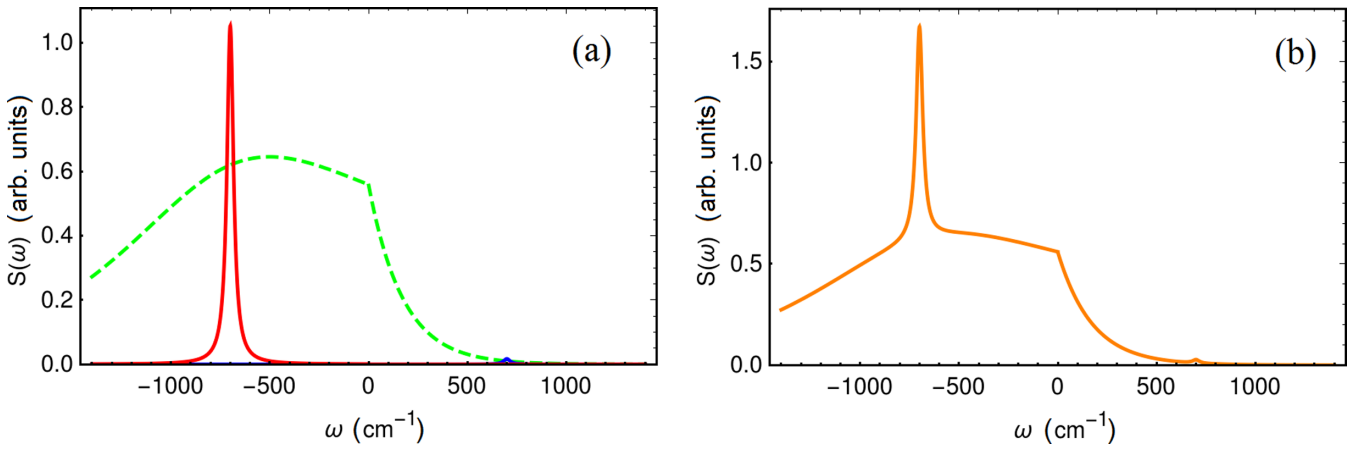


FIG. 1. Spectrum of Raman scattering from a molecule in the presence of a plasmonic nanoantenna. (a) Different components of the spectrum: the Stokes signal from the molecule (solid red line), the anti-Stokes signal from the molecule (blue solid line), the background created by noise in the plasmonic nanoantenna (dashed green line). (b) Total scattering spectrum from the system. The spectrum of Rayleigh scattering is not shown.

we therefore neglect the noise in the electronic subsystem. For a vibrational subsystem, both the ratio $\hbar\omega_{\rm v}/k_{\rm B}T$ and the value of $\bar{n}_{\rm v}^{\rm th}$ can be either greater or less than unity. For this reason, we will retain the noise in the vibrational subsystem.

We also note that the noise and losses in the plasmonic nanoantenna can be divided into three parts: $\hat{F}_a(t) = \hat{F}_a^{\rm rad}(t) + \hat{F}_a^{\rm nonrad}(t) + \hat{a}\hat{F}_a^{\rm Bg}(t)$ and $\gamma_a = \gamma_a^{\rm rad} + \gamma_a^{\rm nonrad} + \gamma_a^{\rm Bg}$. The "rad" index denotes radiative noise and losses, whereas the "nonrad" index denotes nonradiative Joule losses and corresponding noise. The sources of noise describing the radiative and nonradiative Joule losses are related to the corresponding relaxation rates through the relations $\langle \hat{F}_a^{\dagger({\rm non})\rm rad}(t)\hat{F}_a^{({\rm non})\rm rad}(t')\rangle = \gamma_a^{({\rm non})\rm rad}\bar{n}_a^{({\rm non})\rm rad}\delta(t-t')$, where $\bar{n}_a^{({\rm non})\rm rad} = [\exp(\hbar\omega_a/k_{\rm B}T^{({\rm non})\rm rad}) - 1]^{-1}$ represents the average number of quanta in the (non)radiative reservoir. Since at optical frequencies at room temperature the ratio $\hbar\omega_a/k_{\rm B}T^{({\rm non})\rm rad} \gg 1$, then $\bar{n}_a^{({\rm non})\rm rad} \ll 1$. We will therefore neglect the sources of noise $\hat{F}_a^{\rm rad}(t)$ and $\hat{F}_a^{\rm nonrad}(t)$ in the nanoantenna.

Finally, $\hat{F}_a^{\rm Bg}(t)$ and $\gamma_a^{\rm Bg}$ represent the noise and loss associated with the interaction of the electric field in the nanoantenna with phonons. The latter are responsible for the broad luminescent background (hereinafter referred to as the background) of the nanoantenna, the intensity of which is comparable to that of the SERS spectra [47]. However, a rigorous calculation of the noise is not possible, due to the large number of degrees of freedom, and we will therefore proceed as follows. We will assume that the correlation properties of the noise $\hat{F}_a^{\rm Bg}(t)$ are such that the spectrum of a single plasmonic nanoantenna reproduces the experimentally observed shape of the spectrum [41–47]. More specifically, we will assume that the frequency components of the noise $\hat{f}_a^{\rm Bg}(\nu)$ have the following correlation properties:

$$\left\langle \hat{f}_a^{\rm Bg}(\nu)^\dagger \hat{f}_a^{\rm Bg}(\nu')\right\rangle = J_{Bg}(\nu)\delta(\nu-\nu') \tag{5}$$

where

$$\hat{F}_a^{\rm Bg}(t) = \int_{-\infty}^{+\infty} \hat{f}_a^{\rm Bg}(\nu)e^{-i\nu t}d\nu \tag{6}$$

The factor $\hat{a}$ before $\hat{F}_a^{\rm Bg}(t)$ in the expression $\hat{F}_a(t) = \hat{F}_a^{\rm rad}(t) + \hat{F}_a^{\rm nonrad}(t) + \hat{a}\hat{F}_a^{\rm Bg}(t)$ for the total noise in the plasmonic nanoantenna $\hat{F}_a(t)$ reflects the fact that the intensity and characteristic frequencies of the spectrum of the luminescent background of the plasmonic nanoantenna depend on the intensity and frequency of the incident field [41–47]. We note once again that we choose the quantity $J_{\rm Bg}(\nu)$ in a phenomenological way, such that it describes the shape of the luminescent background observed from experiment [41–47] (see also Fig. 1).

We now find a stationary solution to Eqs. (2)–(4). To do this, we apply perturbation theory, assuming that the parameters $\Omega_{{\rm R}j}/|\omega_\sigma - \omega_\Omega|$ and $g/|\omega_\sigma - \omega_\Omega|$ are both small and expanding the operators $\hat{a}$, $\hat{\sigma}_j$, and $\hat{b}_j$ as a series in terms of these small parameters. This theory was developed in [76], and we give only the final expressions here.

According to perturbation theory, there are only thermal vibrations of the nuclei of molecules in the zeroth order:

$$\hat{b}_{j\rm th}(t) = \int_0^t dt' \exp\left[(-i\omega_{\rm v} - \gamma_{\rm v})(t-t')\right]\hat{F}_{b_j}(t'). \tag{7}$$

The average number of quanta of thermal vibrations is determined by the temperature of the vibrational reservoir:

$$\langle \hat{b}_{j\rm th}^\dagger(t)\hat{b}_{i\rm th}(t)\rangle = n_{\rm v}\delta_{ij} = [\exp(\hbar\omega_{\rm v}/k_{\rm B}T) - 1]^{-1}\delta_{ij} \tag{8}$$

In the first order, we obtain a response at the frequency of the external field, which is proportional to the amplitude of the external field,

$$\hat{a}_{\rm R}(t) = \frac{\Omega_{\rm pl}}{(\omega_\Omega - \omega_a) + i\gamma_a}e^{-i\omega_\Omega t}\hat{I},\ \hat{\sigma}_{j\rm R}(t) = \frac{\Omega_{{\rm R}j}}{\omega_\Omega - \omega_\sigma}\hat{a}_{\rm R}(t), \tag{9}$$

and corresponds to Rayleigh scattering. The operator $\hat{a}_{\rm R}(t)$ in Eq. (9) is proportional to the identity operator $\hat{I}$. Here we assume that at the location of the $j$ th molecule, the amplitude of the local field of the plasmonic nanoantenna induced by the external field is much greater than the amplitude of the external field itself.

In the second order, we obtain responses at the Stokes and anti-Stokes frequencies of both molecules and the plasmonic nanoantenna:

$$\begin{aligned}\hat{\sigma}_{j\mathrm{St}}(t) &= \frac{g}{\omega_{\mathrm{St}}-\omega_{\Omega}}\hat{\sigma}_{j\mathrm{R}}(t)\hat{b}^{\dagger}_{j\mathrm{th}}(t),\\ \hat{a}_{\mathrm{St}}(t) &= \frac{\sum_j \Omega_{j\mathrm{R}}\hat{\sigma}_{j\mathrm{St}}(t)}{(\omega_{\mathrm{St}}-\omega_a)+i\gamma_a},\end{aligned} \tag{10}$$

$$\begin{aligned}\hat{\sigma}_{j\mathrm{aSt}}(t) &= \frac{g}{\omega_{\mathrm{aSt}}-\omega_{\Omega}}\hat{\sigma}_{j\mathrm{R}}(t)\hat{b}_{j\mathrm{th}}(t),\\ \hat{a}_{\mathrm{aSt}}(t) &= \frac{\sum_j \Omega_{j\mathrm{R}}\hat{\sigma}_{j\mathrm{aSt}}(t)}{(\omega_{\mathrm{aSt}}-\omega_a)+i\gamma_a},\end{aligned} \tag{11}$$

where we denote the Stokes and anti-Stokes frequencies of the molecule as $\omega_{\mathrm{St}} = \omega_{\Omega} - \omega_{\mathrm{v}}$ and $\omega_{\mathrm{aSt}} = \omega_{\Omega} + \omega_{\mathrm{v}}$, respectively. In addition, we obtain the luminescent background of the nanoantenna:

$$\hat{a}_{\mathrm{Bg}}(t) = \hat{a}_{\mathrm{R}}(t)\int_{-\infty}^{+\infty}\frac{i\hat{f}_a^{\mathrm{Bg}}(\nu)e^{-ivt}}{(v+\omega_{\Omega}-\omega_a)+i\gamma_a}dv. \tag{12}$$

## III. EMISSION SPECTRUM OF A PLASMON NANOANTENNA FED BY A RAMAN SCATTERED SIGNAL FROM A MOLECULE

Since the dipole moment of the plasmonic nanoantenna $d_{\mathrm{pl}}$ is several orders of magnitude greater than the dipole moment of the electronic transition of the molecule $d_{eg}$, we neglect the contribution of light scattered from the molecule to the total spectrum for the system [36]. In this approximation, to calculate the total scattering spectrum for the system, it is sufficient to calculate the spectrum of the light scattered from the plasmonic nanoantenna. According to the Wiener-Khinchin theorem [62,79], the emission spectrum of a plasmonic nanoantenna is expressed in terms of the two-time autocorrelation function of its dipole moment:

$$S(\omega) = |d_{\mathrm{pl}}|^2\mathrm{Re}\int_0^{+\infty}\langle\hat{a}^{\dagger}(t+\tau)\hat{a}(t)\rangle e^{-i\omega\tau}d\tau. \tag{13}$$

To calculate the spectrum in (13), we use the solution for the dipole moment of the nanoantenna in the form $\hat{a} \approx \hat{a}_{\mathrm{R}} + \hat{a}_{\mathrm{St}} + \hat{a}_{\mathrm{aSt}} + \hat{a}_{\mathrm{Bg}}$. From the explicit form of solutions (9)–(12) it follows that the correlators $\langle\hat{a}^{\dagger}_{\mathrm{R}}\hat{a}_{\mathrm{R}}\rangle$, $\langle\hat{a}^{\dagger}_{\mathrm{St}}\hat{a}_{\mathrm{St}}\rangle$, $\langle\hat{a}^{\dagger}_{\mathrm{aSt}}\hat{a}_{\mathrm{aSt}}\rangle$, and $\langle\hat{a}^{\dagger}_{\mathrm{Bg}}\hat{a}_{\mathrm{Bg}}\rangle$ are nonzero, while the cross correlators $\langle\hat{a}^{\dagger}_{\mathrm{St}}\hat{a}_{\mathrm{R}}\rangle$, $\langle\hat{a}^{\dagger}_{\mathrm{aSt}}\hat{a}_{\mathrm{R}}\rangle$, $\langle\hat{a}^{\dagger}_{\mathrm{Bg}}\hat{a}_{\mathrm{R}}\rangle$, $\langle\hat{a}^{\dagger}_{\mathrm{St}}\hat{a}_{\mathrm{aSt}}\rangle$, $\langle\hat{a}^{\dagger}_{\mathrm{St}}\hat{a}_{\mathrm{Bg}}\rangle$, and $\langle\hat{a}^{\dagger}_{\mathrm{aSt}}\hat{a}_{\mathrm{Bg}}\rangle$ are equal to zero. This means that in the scattering spectrum from the system, the intensities of the Rayleigh, Stokes, and anti-Stokes responses and the luminescent background of the plasmonic nanoantenna are added independently. Moreover, due to the independence of the vibrational thermal noises in different molecules [see (8)], Raman signals from different molecules will also appear independently in the general expression for the spectrum. This means that the scattering spectrum in (13) for the system can be represented in the form

$$S(\omega) = S_{\mathrm{R}}(\omega) + \sum_j S_{\mathrm{St}j}(\omega) + \sum_j S_{\mathrm{aSt}j}(\omega) + S_{\mathrm{Bg}}(\omega), \tag{14}$$

where

$$S_{\mathrm{R}}(\omega) = |d_{\mathrm{pl}}|^2\delta(\omega-\omega_{\Omega})\left(\frac{\Omega_{\mathrm{pl}}^2}{(\omega_{\Omega}-\omega_a)^2+\gamma_a^2}\right), \tag{15}$$

$$S_{\mathrm{St}j}(\omega) = \left(\frac{|d_{\mathrm{pl}}|^2\gamma_{\mathrm{v}}(1+n_{\mathrm{v}})}{(\omega_{\mathrm{St}}-\omega)^2+\gamma_{\mathrm{v}}^2}\right)\left(\frac{\Omega_{\mathrm{pl}}^2}{(\omega_{\Omega}-\omega_a)^2+\gamma_a^2}\right)\left(\frac{\Omega_{\mathrm{R}j}^2}{(\omega_{\mathrm{St}}-\omega_a)^2+\gamma_a^2}\right)\left(\frac{g^2}{(\omega_{\mathrm{St}}-\omega_{\sigma})^2}\right)\left(\frac{\Omega_{\mathrm{R}j}^2}{(\omega_{\Omega}-\omega_{\sigma})^2}\right), \tag{16}$$

$$S_{\mathrm{aSt}j}(\omega) = \left(\frac{|d_{\mathrm{pl}}|^2\gamma_{\mathrm{v}}n_{\mathrm{v}}}{(\omega_{\mathrm{aSt}}-\omega)^2+\gamma_{\mathrm{v}}^2}\right)\left(\frac{\Omega_{\mathrm{pl}}^2}{(\omega_{\Omega}-\omega_a)^2+\gamma_a^2}\right)\left(\frac{\Omega_{\mathrm{R}j}^2}{(\omega_{\mathrm{aSt}}-\omega_a)^2+\gamma_a^2}\right)\left(\frac{g^2}{(\omega_{\mathrm{aSt}}-\omega_{\sigma})^2}\right)\left(\frac{\Omega_{\mathrm{R}j}^2}{(\omega_{\Omega}-\omega_{\sigma})^2}\right), \tag{17}$$

$$S_{\mathrm{Bg}}(\omega) = \left(\frac{|d_{\mathrm{pl}}|^2 J_{\mathrm{Bg}}(\omega-\omega_{\Omega})}{(\omega-\omega_a)^2+\gamma_a^2}\right)\left(\frac{\Omega_{\mathrm{pl}}^2}{(\omega_{\Omega}-\omega_a)^2+\gamma_a^2}\right). \tag{18}$$

In expressions (16)–(18), the factors in front of the square brackets determine the dependence of the spectrum on the frequency, and the expression in all but the first parentheses represents the frequency-independent coefficients that determine the total intensity of the scattered light. Expression (15) determines the spectrum of Rayleigh scattering. It can be seen that it is a $\delta$ function, which reflects the fact that Rayleigh scattering is elastic. The terms in (16) and (17) represent the responses from the plasmonic nanoantenna at the Stokes and anti-Stokes frequencies, respectively. In this case, the spectrum of the Stokes and anti-Stokes components is a Lorentz line with a width equal to the decay rate of the vibrations of the nuclei of the molecule (Fig. 1, red and blue solid lines). The ratio of the intensities of the Stokes and anti-Stokes components is equal to $n_{\mathrm{v}}/(n_{\mathrm{v}}+1) = \exp(-\hbar\omega_{\mathrm{v}}/k_{\mathrm{B}}T)$, which is consistent with the results of the experiment reported in [80]. It should be emphasized that expressions (16) and (17) determine the response amplified by the nanoantenna. Its intensity is in the square of the Purcell factor greater than the intensity of the Stokes radiation of a single molecule [81] [see also Eq. (20) in [76]]. In the theory presented here, the Purcell factor $F_{\mathrm{P}j}$ can be written explicitly as $F_{\mathrm{P}j} = \Omega_{\mathrm{R}j}^2/\gamma_a\gamma_{\sigma}$ (a similar definition of the Purcell factor is presented, for example, in [82]). The spectrum of the luminescent background of a plasmonic nanoantenna is the product of the spectral function $J_{\mathrm{Bg}}(\omega-\omega_{\Omega})$ and the plasmon resonance line (for more details, see [47]).

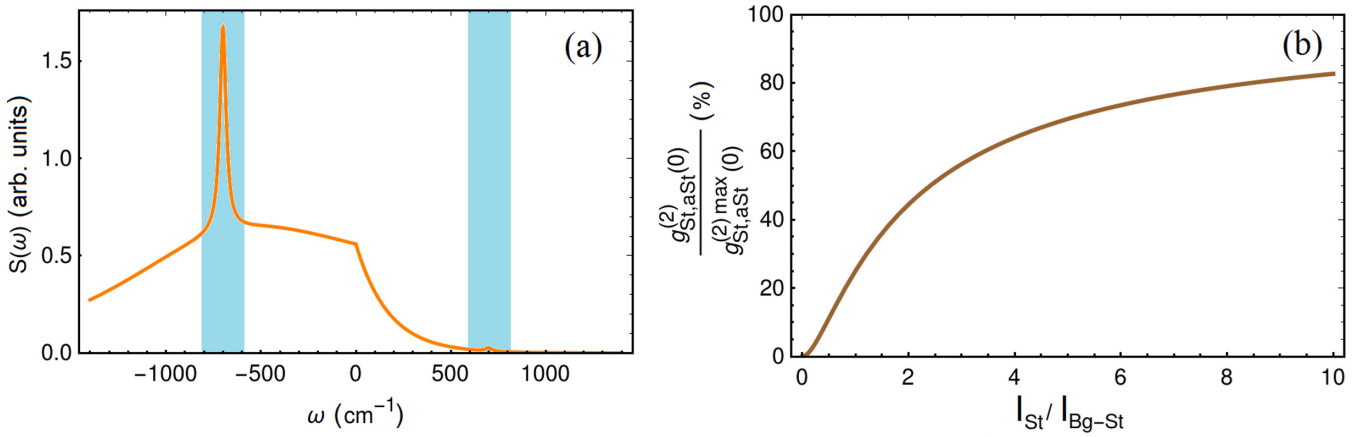


FIG. 2. (a) Scattering spectrum from the system without the Rayleigh contribution. The areas of the spectrum for detecting Stokes and anti-Stokes light are indicated as blue region. (b) Dependence of the ratio of the second-order cross-correlation function to the maximum possible value as a function of the ratio of the intensity of the Stokes signal from the molecule to the background signal from the plasmonic nanoantenna.

Figure 1(a) shows a typical form of the scattering spectrum from molecules placed near a plasmonic nanoantenna [51]. In addition to Rayleigh scattering, the spectrum has a Stokes component [Fig. 1(a), red line, Eq. (16)], an anti-Stokes component [Fig. 1(a), blue line, Eq. (17)], and a luminescence spectrum [Fig. 1(a), green dashed line, Eq. (18)]. Figure 1(b) shows the full spectrum of scattering from the system, as determined by expression (14).

## IV. CROSS CORRELATIONS OF STOKES AND ANTI-STOKES LIGHT

In recent experimental studies [1–6], it was found that the Raman scattered light is nonclassical [7,62]. This nonclassicality arises because the excitation of both Stokes and anti-Stokes photons occurs due to the same vibrations of molecular nuclei. As a result, the Stokes and anti-Stokes photons are emitted in pairs, causing the nonclassical behavior of the mutual second-order coherence function, that is, in violation of the Cauchy-Schwarz inequality $g^{(2)}_{\mathrm{St,aSt}} \leqslant \sqrt{g^{(2)}_{\mathrm{St}} g^{(2)}_{\mathrm{aSt}}}$.

The cross correlations of the Stokes and anti-Stokes radiation from the molecule are described by the second-order correlation function [83]

$$g^{(2)}_{\mathrm{St,aSt}}(0) = \frac{\langle \hat{A}^{\dagger}_{\mathrm{St}}(t)\hat{A}^{\dagger}_{\mathrm{aSt}}(t)\hat{A}_{\mathrm{aSt}}(t)\hat{A}_{\mathrm{St}}(t)\rangle}{\langle \hat{A}^{\dagger}_{\mathrm{St}}(t)\hat{A}_{\mathrm{St}}(t)\rangle \langle \hat{A}^{\dagger}_{\mathrm{aSt}}(t)\hat{A}_{\mathrm{aSt}}(t)\rangle}. \tag{19}$$

Note that the operators $\hat{A}_{\mathrm{St}}(t)$ and $\hat{A}_{\mathrm{aSt}}(t)$ in (19) correspond only to those parts of the SERS spectrum that lie in the frequency ranges near $\omega_{\mathrm{St}} = \omega_{\Omega} - \omega_{\mathrm{v}}$ and $\omega_{\mathrm{aSt}} = \omega_{\Omega} + \omega_{\mathrm{v}}$, respectively [see Fig. 2(a)]. According to the spectral theory of operators developed in [84], the explicit expression for the operators $\hat{A}_{\mathrm{St}}(t)$ and $\hat{A}_{\mathrm{aSt}}(t)$ has the form

$$\hat{A}_{\mathrm{St}}(t) = \frac{1}{2\pi}\int_{\omega_{\mathrm{St}}-3\gamma_{\mathrm{v}}}^{\omega_{\mathrm{St}}+3\gamma_{\mathrm{v}}} d\omega e^{-i\omega t}\int_{-\infty}^{+\infty} dt' e^{i\omega t'}\hat{a}(t'), \tag{20}$$

$$\hat{A}_{\mathrm{aSt}}(t) = \frac{1}{2\pi}\int_{\omega_{\mathrm{aSt}}-3\gamma_{\mathrm{v}}}^{\omega_{\mathrm{aSt}}+3\gamma_{\mathrm{v}}} d\omega e^{-i\omega t}\int_{-\infty}^{+\infty} dt e^{i\omega t'}\hat{a}(t'). \tag{21}$$

By substituting the operator $\hat{a}(t)$ in the form $\hat{a}(t) \approx \hat{a}_{\mathrm{R}}(t) + \hat{a}_{\mathrm{St}}(t) + \hat{a}_{\mathrm{aSt}}(t) + \hat{a}_{\mathrm{Bg}}(t)$ into expressions (20) and (21), and taking into account (9)–(12), we obtain approximate expressions for the operators $\hat{A}_{\mathrm{St}}(t)$ and $\hat{A}_{\mathrm{aSt}}(t)$:

$$\hat{A}_{\mathrm{St}}(t) \approx \hat{a}_{\mathrm{St}}(t) + \hat{a}_{\mathrm{R}}(t)\int_{\omega_{\mathrm{St}}-3\gamma_{\mathrm{v}}}^{\omega_{\mathrm{St}}+3\gamma_{\mathrm{v}}} \frac{i\hat{f}_a(\omega-\omega_{\Omega})}{(\omega-\omega_a)+i\gamma_a} e^{-i(\omega-\omega_{\Omega})t} d\omega, \tag{22}$$

$$\hat{A}_{\mathrm{aSt}}(t) = \hat{a}_{\mathrm{aSt}}(t) + \hat{a}_{\mathrm{R}}(t)\int_{\omega_{\mathrm{aSt}}-3\gamma_{\mathrm{v}}}^{\omega_{\mathrm{aSt}}+3\gamma_{\mathrm{v}}} \frac{i\hat{f}_a(\omega-\omega_{\Omega})}{(\omega-\omega_a)+i\gamma_a} e^{-i(\omega-\omega_{\Omega})t} d\omega. \tag{23}$$

The explicit forms of the operators in (22) and (23) can be used to calculate the cross-correlation function of the second order (19). Substitution of (22) and (23) into (19) gives

$$g^{(2)}_{\mathrm{St,aSt}}(0) = 1 + \frac{1+n_{\mathrm{v}}}{n_{\mathrm{v}}}\frac{1}{(1+I_{\mathrm{Bg\text{-}St}}/I_{\mathrm{St}})(1+I_{\mathrm{Bg\text{-}aSt}}/I_{\mathrm{aSt}})}, \tag{24}$$

where $I_{\mathrm{St}}$, $I_{\mathrm{aSt}}$, $I_{\mathrm{Bg\text{-}St}}$, and $I_{\mathrm{Bg\text{-}aSt}}$ are defined as

$$I_{\mathrm{St}} = \int_{\omega_{\mathrm{St}}-3\gamma_{\mathrm{v}}}^{\omega_{\mathrm{St}}+3\gamma_{\mathrm{v}}} \sum_j S_{\mathrm{St}j}(\omega) d\omega, \tag{25}$$

$$I_{\mathrm{aSt}} = \int_{\omega_{\mathrm{aSt}}-3\gamma_{\mathrm{v}}}^{\omega_{\mathrm{aSt}}+3\gamma_{\mathrm{v}}} \sum_j S_{\mathrm{aSt}j}(\omega) d\omega, \tag{26}$$

$$I_{\text{Bg-St}} = \int_{\omega_{\text{St}}-3\gamma_{\text{v}}}^{\omega_{\text{St}}+3\gamma_{\text{v}}} S_{\text{Bg}}(\omega)d\omega, \tag{27}$$

$$I_{\text{Bg-aSt}} = \int_{\omega_{\text{aSt}}-3\gamma_{\text{v}}}^{\omega_{\text{aSt}}+3\gamma_{\text{v}}} S_{\text{Bg}}(\omega)d\omega. \tag{28}$$

As noted above, we choose the quantity $J_{\text{Bg}}(\nu)$ in a phenomenological way to describe the shape of the luminescent background observed experimentally [41–47]. If we assume that $J_{\text{Bg}}(-\nu) = \exp(-\hbar\nu/k_{\text{B}}T)J_{\text{Bg}}(\nu)$, then from expressions (25)–(28) and (16)–(18) we obtain that the ratio of the background to the Raman signal from the molecule in the anti-Stokes part of the spectrum coincides with the ratio of the background to the Raman signal from the molecule in the Stokes part of the spectrum, $I_{\text{St}}/I_{\text{Bg-St}} = I_{\text{aSt}}/I_{\text{Bg-aSt}}$. This result is consistent with experimental data [79].

In the absence of a background signal from the plasmonic nanoantenna, $I_{\text{Bg-St}} = I_{\text{Bg-aSt}} = 0$, the cross-correlation function of the second order (24) reaches its maximum value $g^{(2)\,\max}_{\text{St,aSt}}(0) = 1 + (1 + n_{\text{v}})/n_{\text{v}}$. Figure 2 shows a decrease in the cross-correlation function of the second order $g^{(2)}_{\text{St,aSt}}(0)$ as a function of the ratio of the intensities of the Stokes signal from the molecule to the noise signal from the plasmonic nanoantenna $I_{\text{St}}/I_{\text{Bg-St}}$.

## V. INFLUENCE OF THE GEOMETRY OF THE PLASMONIC NANOANTENNA ON THE CORRELATIONS OF STOKES AND ANTI-STOKES LIGHT

In the previous section, we showed that the higher the values $I_{\text{St}}/I_{\text{Bg-St}}$ and $I_{\text{aSt}}/I_{\text{Bg-aSt}}$, the closer the second-order cross-correlation function $g^{(2)}_{\text{St,aSt}}(0)$ to its maximum possible value $g^{(2)\,\max}_{\text{St,aSt}}(0)$ [see expression (24) and Fig. 2]. On the other hand, for practical applications, not only is the value of the second-order autocorrelation function, $g^{(2)}_{\text{St,aSt}}(0)$, important, but also the absolute values of the intensities of the Stokes and anti-Stokes signals, $I_{\text{St}}$ and $I_{\text{aSt}}$. In this section, we investigate the question of whether it is possible, by changing the geometry of the plasmonic nanoantenna, to increase the second-order cross-correlation function $g^{(2)}_{\text{St,aSt}}(0)$ while maintaining a high intensity of the Raman signals $I_{\text{St}}$ and $I_{\text{aSt}}$.

It follows from expressions (25), (26) and (16), (17) that regardless of the geometry and size of the plasmonic nanoantenna, the intensities of the Stokes and anti-Stokes signals are

$$I_{\text{aSt}} \propto I_{\text{St}} \propto N \times \left(\frac{\gamma_a^{\text{rad}}}{\gamma_a}\right)^2 \times \frac{\Omega_{\text{R}}^2}{\gamma_a} \times \frac{\Omega_{\text{R}}^2}{\gamma_a} \propto N(\eta F_{\text{P}})^2, \tag{29}$$

where $\eta$ is the quantum yield of the plasmonic nanoantenna, determined by the ratio of the rate of radiative losses in the nanoantenna $\gamma_a^{\text{rad}}$ to the rate of total losses in the plasmonic nanoantenna $\gamma_a$, $\eta = \gamma_a^{\text{rad}}/\gamma_a$; $F_{\text{P}}$ is the characteristic value of the Purcell factor for molecules located near the plasmonic nanoantenna; and $N$ is the number of molecules that effectively interact with the plasmonic nanoantenna.

Similarly, it follows from expressions (27), (28), and (18) that the expression for the photoluminescence intensity of a plasmonic nanoantenna is

$$I_{\text{Bg-St}} \propto \frac{J(\omega_{\text{St}} - \omega_\Omega)}{\gamma_a^2}\left(\frac{\gamma_a^{\text{rad}}}{\gamma_a}\right)^2 = \frac{J(\omega_{\text{St}} - \omega_\Omega)}{\gamma_a^2}\eta^2, \tag{30}$$

$$I_{\text{Bg-aSt}} \propto \frac{J(\omega_{\text{aSt}} - \omega_\Omega)}{\gamma_a^2}\left(\frac{\gamma_a^{\text{rad}}}{\gamma_a}\right)^2 = \frac{J(\omega_{\text{aSt}} - \omega_\Omega)}{\gamma_a^2}\eta^2. \tag{31}$$

Using expressions (29)–(31) we will consider ways of increasing the cross-correlation function of the second order of the Stokes and anti-Stokes signals while simultaneously maintaining a high intensity of the Raman signal. To achieve this goal, we can attempt to optimize both the size and the shape of the plasmonic nanoantenna.

First, we consider the possibility of optimizing the size of the plasmonic nanoantenna. For simplicity, we consider a spherical plasmonic nanoantenna of radius $R$. The factors included in expression (29) depend on the radius of the plasmonic nanoparticle, according to $\eta = \gamma_a^{\text{rad}}/\gamma_a = R^3/(R^3 + R_{\text{rad}}^3)$ and $F_{\text{P}} = \Omega_{\text{R}}^2/\gamma_a\gamma_\sigma \sim R_{\text{rad}}^6/R^3(R^3 + R_{\text{rad}}^3)$ [75]. We denote the radius of the plasmonic nanoantenna, for which the radiative losses are compared with the nonradiative ones [85,86], as $R_{\text{rad}}$. For a plasmonic nanoantenna made of gold, the characteristic size $R_{\text{rad}}$ is about 50 nm [85,86]. From this and from expression (29) we obtain

$$I_{\text{aSt}} \propto I_{\text{St}} \propto \frac{N}{[1 + (R/R_{\text{rad}})^3]^4}. \tag{32}$$

In an analogous way, for the intensities of the photoluminescent background (30) and (31), we obtain

$$I_{\text{Bg-aSt}} \propto I_{\text{Bg-St}} \propto \frac{1}{[(R/R_{\text{rad}})^3 + 1]^2}\frac{1}{[(R_{\text{rad}}/R)^3 + 1]^2}. \tag{33}$$

Note that the dependence of the number of particles $N$ that effectively interact with the plasmonic nanoantenna on the size of the nanoantenna is determined to a large extent by the experimental design. In some experiments, the system under consideration is a single molecule interacting with a plasmonic nanoantenna [48]. In this case, $N$ equals unity and does not depend on the size of the nanoantenna. In other experiments [87], the plasmon nanoantenna is completely covered by molecules; in this case, the number of molecules effectively interacting with the plasmonic nanoantenna is proportional to the nanoantenna's surface, i.e., $N \propto (R/R_{\text{rad}})^2$, where we introduce $R_{\text{rad}}$ to obtain a dimensionless quantity.

Figure 3 shows the normalized intensities of the Raman signal (32) and the intensities of the luminescent background of the plasmonic nanoantenna (33) as functions of the radius of the spherical plasmonic nanoantenna in the case where one molecule interacts with the nanoantenna. As can be seen from Fig. 3(a), in order to optimize the second-order cross-correlation function, it is necessary to reduce the size of the nanoantenna. At the same time, when the size is reduced, the fluorescent background of the plasmonic nanoantenna is suppressed [see Eq. (33)], and the intensity of the Raman signal increases. This behavior of the Raman signal intensity is consistent with the experimental data presented in [48]. Hence, to achieve both a high intensity and a degree of non-

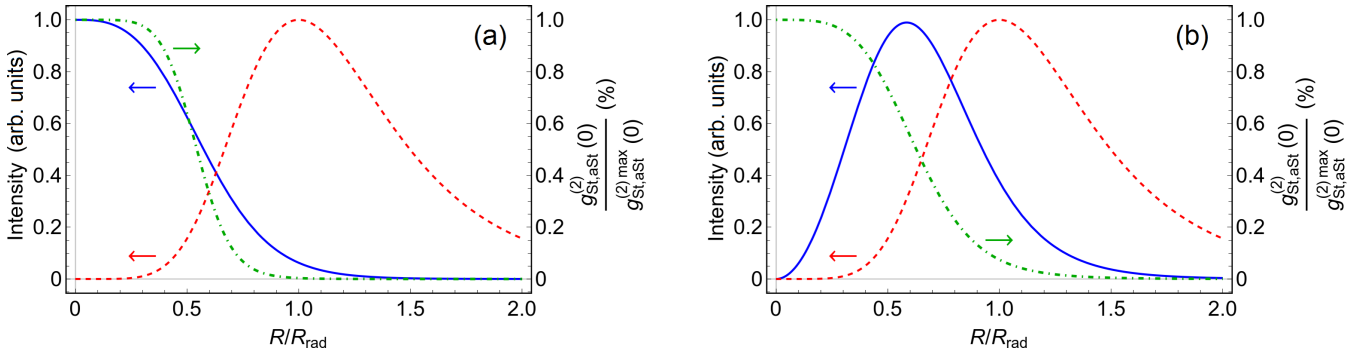


FIG. 3. Normalized values of the intensity of the Raman signal (32) (blue solid line) and the fluorescent background (33) (red dotted line) and ratio of the second-order cross-correlation function to the maximum possible value (green dash-dotted line) depending on the radius of the spherical nanoantenna in the case of a single molecule (a) and many molecules covering nanoantenna (b).

classicality simultaneously, it is necessary to reduce the size of the plasmonic nanoantenna.

Figure 3(b) shows the dependence of the intensity of the Raman signal and the intensity of the fluorescent background of the plasmonic nanoantenna on the radius of the nanoantenna, in the case where the molecules completely cover the nanoantenna. In this case, the optimal radius of the plasmonic nanoantenna at which a high intensity and a degree of nonclassicality are achieved simultaneously is about $0.5R_{\rm rad}$.

We now analyze the way in which the shape of the plasmonic nanoantenna affects the second-order cross-correlation function of the Stokes and anti-Stokes signals and the intensities of these signals. A change in its shape leads to a change in the volume of the mode [88]. By changing the shape of the plasmonic nanoantenna, it is possible to create a so-called "hot spot," i.e., a distribution of the electric field strength of the eigenmode of the plasmonic nanoantenna in which the field is concentrated within a small volume. For example, a hot spot can be implemented in a plasmonic nanoantenna composed of two spherical nanoparticles located close to each other [48]. Let the shape of the plasmonic nanoantenna be chosen so that the volume of the mode is equal to $V$. As can be seen from formulas (30) and (31) the intensity of the photoluminescent background of the plasmon nanoantenna does not depend on $V$; however, the intensity of the Raman signal (29) is proportional to the square of the Purcell factor, and therefore does depend on $V$. The Purcell factor for a molecule in a hot spot is inversely proportional to the volume of the plasmonic nanoantenna mode, $F_{\rm P} \propto 1/V$ [89]. In this case, the intensity of the Raman signal, according to (29), is proportional to the following ratio:

$$I_{\rm aSt} \propto I_{\rm St} \propto \frac{N}{V}. \tag{34}$$

From expression (34) we can conclude that a decrease in the volume of a plasmonic nanoantenna mode does not lead to an increase in the Raman signal intensity if the hot spot is completely filled with molecules. In this case, the number of molecules effectively interacting with the plasmonic nanoantenna is determined by the concentration of these molecules $n$ according to $N = nV$, where $V$ is the volume of the plasmonic nanoantenna mode. Thus, the magnitude of the Raman signal ceases to depend on the volume of the plasmonic nanoantenna mode when the molecules occupy the hot spot in a uniform way.

The situation is quite different when we consider a single molecule placed in a hot spot [48,90]. In this case (34) $N = 1$ and the intensity of the Raman signal turns out to be inversely proportional to the volume of the plasmonic nanoantenna mode. Thus, in the case of the interaction of a single molecule with a plasmonic nanoantenna, it turns out to be advantageous to decrease the volume of the plasmonic nanoantenna mode and to place the molecule within a hot spot.

## VI. CONCLUSION

We consider the influence of a plasmonic nanoantenna on the cross correlations of the Stokes and anti-Stokes signals from a molecule placed near the plasmonic nanoantenna. It is shown that the plasmonic nanoantenna decreases the second-order cross-correlation functions for the Stokes and anti-Stokes signals. This decrease is due to the presence of a background signal from the plasmonic nanoantenna. It is found that there is a size of the nanoantenna for which nonclassical correlations are preserved and the emitted signal is amplified, as in SERS experiments. It is also shown that in the case where the plasmonic nanoantenna is completely covered with molecules, its optimal size is about half the size at which the radiative losses of the plasmonic nanoantenna are comparable with the nonradiative ones. At the optimal size of the plasmonic nanoantenna, the cross-correlation functions of the second order for the Stokes and anti-Stokes signals increase, and the intensities of these signals reach a maximum value. For the case where a single molecule interacts with the plasmonic nanoantenna, the geometry of the plasmonic nanoantenna can be optimized by both reducing the size of the nanoantenna and decreasing the volume of its mode. This result can be used to increase the intensity of paired photon sources based on spontaneous Raman light scattering.

## ACKNOWLEDGMENTS

The study was supported by a grant from Russian Science Foundation (Project No. 20-72-10057). E.S.A. thanks the Foundation for the Advancement of Theoretical Physics and Mathematics "Basis."

[1] K. C. Lee, B. J. Sussman, M. R. Sprague, P. Michelberger, K. F. Reim, J. Nunn, N. K. Langford, P. J. Bustard, D. Jaksch, and I. A. Walmsley, Macroscopic non-classical states and terahertz quantum processing in room-temperature diamond, Nat. Photonics **6**, 41 (2012).

[2] M. Kasperczyk *et al.*, Stokes–anti-Stokes correlations in diamond, Opt. Lett. **40**, 2393 (2015).

[3] F. S. de Aguiar Júnior *et al.*, Lifetime and polarization for real and virtual correlated Stokes-anti-Stokes Raman scattering in diamond, Phys. Rev. Res. **2**, 013084 (2020).

[4] M. Kasperczyk *et al.*, Temporal Quantum Correlations in Inelastic Light Scattering from Water, Phys. Rev. Lett. **117**, 243603 (2016).

[5] A. Saraiva *et al.*, Photonic Counterparts of Cooper Pairs, Phys. Rev. Lett. **119**, 193603 (2017).

[6] M. D. Anderson *et al.*, Two-Color Pump-Probe Measurement of Photonic Quantum Correlations Mediated by a Single Phonon, Phys. Rev. Lett. **120**, 233601 (2018).

[7] R. Loudon, *The Quantum Theory of Light* (Oxford University Press, Oxford, 2000).

[8] T. B. Pittman *et al.*, Optical imaging by means of two-photon quantum entanglement, Phys. Rev. A **52**, R3429 (1995).

[9] T. Pittman *et al.*, Two-photon geometric optics, Phys. Rev. A **53**, 2804 (1996).

[10] M. N. O'Sullivan, K. W. C. Chan, and R. W. Boyd, Comparison of the signal-to-noise characteristics of quantum versus thermal ghost imaging, Phys. Rev. A **82**, 053803 (2010).

[11] R. I. Khakimov *et al.*, Ghost imaging with atoms, Nature (London) **540**, 100 (2016).

[12] N. Sangouard *et al.*, Quantum repeaters based on atomic ensembles and linear optics, Rev. Mod. Phys. **83**, 33 (2011).

[13] C. Chou *et al.*, Single-Photon Generation from Stored Excitation in an Atomic Ensemble, Phys. Rev. Lett. **92**, 213601 (2004).

[14] S. Chen *et al.*, Deterministic and Storable Single-Photon Source Based on a Quantum Memory, Phys. Rev. Lett. **97**, 173004 (2006).

[15] J. Laurat *et al.*, Efficient retrieval of a single excitation stored in an atomic ensemble, Opt. Express **14**, 6912 (2006).

[16] D. Matsukevich *et al.*, Deterministic Single Photons via Conditional Quantum Evolution, Phys. Rev. Lett. **97**, 013601 (2006).

[17] H. De Riedmatten *et al.*, Direct Measurement of Decoherence for Entanglement Between a Photon and Stored Atomic Excitation, Phys. Rev. Lett. **97**, 113603 (2006).

[18] S. Chen *et al.*, Demonstration of a Stable Atom-Photon Entanglement Source for Quantum Repeaters, Phys. Rev. Lett. **99**, 180505 (2007).

[19] D. Felinto *et al.*, Conditional control of the quantum states of remote atomic memories for quantum networking, Nat. Phys. **2**, 844 (2006).

[20] Z.-S. Yuan *et al.*, Synchronized Independent Narrow-Band Single Photons and Efficient Generation of Photonic Entanglement, Phys. Rev. Lett. **98**, 180503 (2007).

[21] J. Laurat *et al.*, Heralded entanglement between atomic ensembles: Preparation, decoherence, and scaling, Phys. Rev. Lett. **99**, 180504 (2007).

[22] P.-Y. Chen, C. Argyropoulos, and A. Alù, Enhanced nonlinearities using plasmonic nanoantennas, Nanophotonics **1**, 221 (2012).

[23] T. B. Hoang *et al.*, Ultrafast spontaneous emission source using plasmonic nanoantennas, Nat. Commun. **6**, 1 (2015).

[24] A. F. Koenderink, Single-photon nanoantennas, ACS Photonics **4**, 710 (2017).

[25] A. E. Krasnok *et al.*, An antenna model for the Purcell effect, Sci. Rep. **5**, 12956 (2015).

[26] M. Nafari and J. M. Jornet, Modeling and performance analysis of metallic plasmonic nano-antennas for wireless optical communication in nanonetworks, IEEE Access **5**, 6389 (2017).

[27] M. Schnell *et al.*, Controlling the near-field oscillations of loaded plasmonic nanoantennas, Nat. Photonics **3**, 287 (2009).

[28] S. Simoncelli *et al.*, Quantitative single-molecule surface-enhanced Raman scattering by optothermal tuning of DNA origami-assembled plasmonic nanoantennas, ACS Nano **10**, 9809 (2016).

[29] T. H. Taminiau, F. Stefani, and N. F. van Hulst, Single emitters coupled to plasmonic nano-antennas: Angular emission and collection efficiency, New J. Phys. **10**, 105005 (2008).

[30] S.-Y. Ding *et al.*, Electromagnetic theories of surface-enhanced Raman spectroscopy, Chem. Soc. Rev. **46**, 4042 (2017).

[31] H. Xu *et al.*, Spectroscopy of Single Hemoglobin Molecules by Surface Enhanced Raman Scattering, Phys. Rev. Lett. **83**, 4357 (1999).

[32] W. Fang *et al.*, Quantizing single-molecule surface-enhanced Raman scattering with DNA origami metamolecules, Sci. Adv. **5**, eaau4506 (2019).

[33] P. Johansson, H. Xu, and M. Käll, Surface-enhanced Raman scattering and fluorescence near metal nanoparticles, Phys. Rev. B **72**, 035427 (2005).

[34] K. Kneipp, M. Moskovits, and H. Kneipp, *Surface-enhanced Raman Scattering: Physics and Applications* (Springer Science & Business Media, New York, 2006), Vol. 103.

[35] J. Langer *et al.*, Present and future of surface-enhanced Raman scattering, ACS Nano **14**, 28 (2019).

[36] S. I. Maslovski and C. R. Simovski, Purcell factor and local intensity enhancement in surface-enhanced Raman scattering, Nanophotonics **8**, 429 (2019).

[37] V. N. Pustovit and T. V. Shahbazyan, Microscopic theory of surface-enhanced Raman scattering in noble-metal nanoparticles, Phys. Rev. B **73**, 085408 (2006).

[38] P. Roelli *et al.*, Molecular cavity optomechanics as a theory of plasmon-enhanced Raman scattering, Nat. Nanotechnol. **11**, 164 (2016).

[39] J. A. Sánchez-Gil and J. Garcıa-Ramos, Calculations of the direct electromagnetic enhancement in surface enhanced Raman scattering on random self-affine fractal metal surfaces, J. Chem. Phys. **108**, 317 (1998).

[40] M. K. Schmidt *et al.*, Linking classical and molecular optomechanics descriptions of SERS, Faraday Discuss. **205**, 31 (2017).

[41] H. Hu *et al.*, Plasmon-modulated photoluminescence of individual gold nanostructures, ACS Nano **6**, 10147 (2012).

[42] D. Huang *et al.*, Photoluminescence of a plasmonic molecule, ACS Nano **9**, 7072 (2015).

[43] C. Lumdee, B. Yun, and P. G. Kik, Gap-plasmon enhanced gold nanoparticle photoluminescence, ACS Photonics **1**, 1224 (2014).

[44] H. Wei *et al.*, Improved quantitative SERS enabled by surface plasmon enhanced elastic light scattering, Anal. Chem. **90**, 3227 (2018).

[45] T. Yin *et al.*, Anomalous shift behaviors in the photoluminescence of dolmen-like plasmonic nanostructures, ACS Photonics **3**, 979 (2016).

[46] R. Zhang *et al.*, Chemical mapping of a single molecule by plasmon-enhanced Raman scattering, Nature (London) **498**, 82 (2013).

[47] V. Y. Shishkov *et al.*, Cascade Brillouin scattering as a mechanism for photoluminescence from rough surfaces of noble metals, Phys. Rev. B **103**, 035408 (2021).

[48] K.-Q. Lin *et al.*, Size effect on SERS of gold nanorods demonstrated via single nanoparticle spectroscopy, J. Phys. Chem. C **120**, 20806 (2016).

[49] R. B. Chevalier and J. R. Dwyer, An open source, iterative dual-tree wavelet background subtraction method extended from automated diffraction pattern analysis to optical spectroscopy, Appl. Spectrosc. **73**, 1370 (2019).

[50] C. Galloway, E. Le Ru, and P. Etchegoin, An iterative algorithm for background removal in spectroscopy by wavelet transforms, Appl. Spectrosc. **63**, 1370 (2009).

[51] K.-Q. Lin *et al.*, Plasmonic photoluminescence for recovering native chemical information from surface-enhanced Raman scattering, Nat. Commun. **8**, 1 (2017).

[52] R. Mallia *et al.*, Filter-based method for background removal in high-sensitivity wide-field-surface-enhanced Raman scattering imaging in vivo, J. Biomed. Opt. **17**, 076017 (2012).

[53] Y. Xie *et al.*, An auto-adaptive background subtraction method for Raman spectra, Spectrochim. Acta, Part A **161**, 58 (2016).

[54] S. I. Bogdanov *et al.*, Ultrafast quantum photonics enabled by coupling plasmonic nanocavities to strongly radiative antennas, Optica **7**, 463 (2020).

[55] T. B. Hoang, G. M. Akselrod, and M. H. Mikkelsen, Ultrafast room-temperature single photon emission from quantum dots coupled to plasmonic nanocavities, Nano Lett. **16**, 270 (2016).

[56] L. Lange *et al.*, Controlling photon antibunching from 1D emitters using optical antennas, Nanoscale **11**, 14907 (2019).

[57] N. Livneh *et al.*, Highly directional room-temperature single photon device, Nano Lett. **16**, 2527 (2016).

[58] S. Schietinger *et al.*, Plasmon-enhanced single photon emission from a nanoassembled metal− diamond hybrid structure at room temperature, Nano Lett. **9**, 1694 (2009).

[59] A. Singh *et al.*, Nanoscale mapping and control of antenna-coupling strength for bright single photon sources, Nano Lett. **18**, 2538 (2018).

[60] N. E. Nefedkin *et al.*, Second-order coherence function of a plasmonic nanoantenna fed by a single-photon source, Opt. Express **27**, 23396 (2019).

[61] A. Lombardi *et al.*, Pulsed Molecular Optomechanics in Plasmonic Nanocavities: From Nonlinear Vibrational Instabilities to Bond-Breaking, Phys. Rev. X **8**, 011016 (2018).

[62] M. O. Scully and M. S. Zubairy, *Quantum Optics* (Cambridge University Press, Cambridge, England, 1997).

[63] M. Born and R. Oppenheimer, On the quantum theory of molecules, in *Quantum Chemistry: Classic Scientific Papers* (World Scientific, Singapore, 2000), pp. 1–24.

[64] H. Köuppel, W. Domcke, and L. S. Cederbaum, Multimode molecular dynamics beyond the Born-Oppenheimer approximation, Adv. Chem. Phys. **57**, 59 (1984).

[65] D. Wigger *et al.*, Quantum dynamics of optical phonons generated by optical excitation of a quantum dot, J. Comput. Electron. **15**, 1158 (2016).

[66] L. Droenner and J. Kabuss, Theory of an optically driven quantum-dot phonon laser, in *Physics and Simulation of Optoelectronic Devices XXIII*, edited by B. Witzigmann, M. Osiski, F. Henneberger, and Y. Arakawa (International Society for Optics and Photonics, San Francisco, California, 2015), p. 372.

[67] N. L. Naumann *et al.*, Solid-state-based analog of optomechanics, J. Opt. Soc. Am. B **33**, 1492 (2016).

[68] J. Kabuss *et al.*, Optically driven quantum dots as source of coherent cavity phonons: A proposal for a phonon laser scheme, Phys. Rev. Lett. **109**, 054301 (2012).

[69] R. Merlin, Generating coherent THz phonons with light pulses, Solid State Commun. **102**, 207 (1997).

[70] J. Kabuss, A. Carmele, and A. Knorr, Threshold behavior and operating regimes of an optically driven phonon laser: Semiclassical theory, Phys. Rev. B **88**, 064305 (2013).

[71] V. Y. Shishkov *et al.*, Connection between vibrational instabilities of molecules in surface-enhanced Raman spectroscopy and Raman lasing, Phys. Rev. A **100**, 053838 (2019).

[72] R. A. Diaz *et al.*, Effective Hamiltonian for Stokes–anti-Stokes pair generation with pump and probe polarized modes, Phys. Rev. B **102**, 134304 (2020).

[73] T. G. Philbin, Canonical quantization of macroscopic electromagnetism, New J. Phys. **12**, 123008 (2010).

[74] V. Y. Shishkov *et al.*, Hermitian description of localized plasmons in dispersive dissipative subwavelength spherical nanostructures, Phys. Rev. B **94**, 235443 (2016).

[75] E. Andrianov *et al.*, Spontaneous radiation of a two-level atom into multipole modes of a plasmonic nanoparticle, Photonics Nanostruct.: Fund. Appl. **12**, 387 (2014).

[76] V. Y. Shishkov *et al.*, Enhancement of the Raman Effect by Infrared Pumping, Phys. Rev. Lett. **122**, 153905 (2019).

[77] M. Reitz, C. Sommer, and C. Genes, Langevin Approach to Quantum Optics with Molecules, Phys. Rev. Lett. **122**, 203602 (2019).

[78] H. Haken, *Laser Light Dynamics* (North-Holland, Amsterdam, 1985), Vol. 1.

[79] J. T. Hugall and J. J. Baumberg, Demonstrating photoluminescence from Au is electronic inelastic light scattering of a plasmonic metal: The origin of SERS backgrounds, Nano Lett. **15**, 2600 (2015).

[80] E. Smith and G. Dent, *Modern Raman Spectroscopy: A Practical Approach* (John Wiley & Sons Ltd, Chichester, England, 2005).

[81] S.-Y. Ding *et al.*, Nanostructure-based plasmon-enhanced Raman spectroscopy for surface analysis of materials, Nat. Rev. Mater. **1**, 1 (2016).

[82] E. Waks and D. Sridharan, Cavity QED treatment of interactions between a metal nanoparticle and a dipole emitter, Phys. Rev. A **82**, 043845 (2010).

[83] R. J. Glauber, The quantum theory of optical coherence, Phys. Rev. **130**, 2529 (1963).

[84] X.-B. Yan *et al.*, Entanglement optimization of filtered output fields in cavity optomechanics, Opt. Express **27**, 24393 (2019).

[85] L. Novotny and B. Hecht, *Principles of Nano-optics* (Cambridge University Press, New York, UK, 2012).

[86] E. Andrianov *et al.*, Dynamics of the transient regime of spaser, J. Commun. Technol. Electron. **56**, 1471 (2011).

[87] L. Qin *et al.*, The strong dependence of the bi-functionalities of core–shell-like gold-based nanocomposites on the size of gold nanoparticles, J. Mater. Chem. C **5**, 11411 (2017).

[88] S. A. Maier, Plasmonic field enhancement and SERS in the effective mode volume picture, Opt. Express **14**, 1957 (2006).

[89] E. M. Purcell, Spontaneous emission probabilities at radio frequencies, Phys. Rev. **69**, 681 (1946).

[90] Y. Zhang, Y. R. Zhen, O. Neumann *et al.*, Coherent anti-Stokes Raman scattering with single-molecule sensitivity using a plasmonic Fano resonance, Nat. Commun. **5**, 4424 (2014).